Available online at www.sciencedirect.com
ScienceDirect
Journal of the Franklin Institute 348 (2011) 1886–1902
Journal of The Franklin Institute
www.elsevier.com/locate/jfranklin

# MIMO fuzzy sliding mode controlled dual arm robot in load transportation

Yuksel Hacioglu, Yunus Ziya Arslan, Nurkan Yagiz*

*Department of Mechanical Engineering, Faculty of Engineering, Istanbul University, 34320 Avcilar, Istanbul, Turkey*

Received 6 May 2009; received in revised form 27 February 2011; accepted 6 May 2011
Available online 17 May 2011

**Abstract**

The control problem of the cooperative motion of a two-link dual arm robot during handling and transportation of an object was studied in this paper. Since these types of robots are frequently preferred for hazardous applications such as transportation of radioactive materials and disposal of explosives, a robust non-chattering sliding mode controller (SMC) improved by a multiple-input multiple-output (MIMO) fuzzy logic unit was applied to the robot to track the desired trajectory with high accuracy and transport the load safely. In order to assess the performance of the proposed MIMO fuzzy sliding mode controller (MIMO-FSMC) in presence of parameter variations and external disturbances, a sudden load variation and noise were introduced to the robot system. If compared with classical SMC, tracking errors with smaller magnitudes and faster convergence to zero were obtained by using the proposed MIMO-FSMC. Numerical results suggest that this type of control method may safely be used for cooperative motion control of dual arm robots in load handling and transport applications in hazardous environments with high accuracy.


## 1. Introduction

The problem of cooperative motion control of dual arm robots has attracted many investigators in recent years [1–6]. The reason of this interest mainly stems from the fact that dual arm robots have certain advantages when compared with the single arm

*Corresponding author. Tel.:+902124737048; fax:+902124737180.
*E-mail addresses:* yukselh@istanbul.edu.tr (Y. Hacioglu), yzarslan@istanbul.edu.tr (Y.Z. Arslan), nurkany@istanbul.edu.tr (N. Yagiz).

0016-0032/$32.00 
doi:10.1016/j.jfranklin.2011.05.009

robots [7–9]. For example, the cooperative dual arm robot systems have a greater capability of handling large objects from the viewpoint of ease of manipulation and higher precision than single arm robots [10]. Both of these essential features should be taken into account while conducting a study on the robot designs for hazardous environment tasks, such as transportation of radioactive materials in nuclear power plants and disposal of explosive ordnances [11]. Moreover, in these types of environments especially when there is a possibility of facing with unexpected disturbances, cooperative motion control of the robot arms during transportation of the load becomes extremely important. Therefore, in these circumstances, a robust controller should be used in order to maintain the desired trajectory of robot arms with high accuracy and safe handling.

Owing to its insensitivity to parameter variations and external disturbances, sliding mode controller (SMC) is preferred in wide range of applications such as control of robotic manipulators [12–14], motion control of mobile robots [15], flight control [16], control of electric drives [17], dynamic positioning control of vessels [18], fault diagnosis for vertical three-tank systems [19], etc. The main drawback of this control method used to be chattering, which is due to the discontinuous part in the control law. On the other hand, it can be solved by using a continuous approximation for the discontinuous part [20] or by designing a continuous control law in the beginning [21].

During the last decades, great effort has been made to improve the transient characteristics of the conventional SMC. Choi et al. proposed a moving switching surface in order to shorten the reaching phase, where the switching surface is initially designed to pass the arbitrary initial conditions and subsequently move towards a predetermined switching surface by rotating and/or shifting [22]. Roy and Olgac expanded the idea of moving switching surface to nth order case [23]. Tokat et al. proposed a nonlinear time-varying sliding surface for the SMC applied on a planar robot which decreased reaching time [24]. Bartoszewicz and Nowacka-Leverton have presented a SMC with a time varying sliding surface for a third order system in presence of acceleration constraint [25]. They obtained fast error convergence to zero. Tokat defined the sliding surface using angular information as a function of time that provided continuous movement of the sliding surface [26]. Bartoszewicz and Nowacka-Leverton have also investigated the case with constraints on input signal [27]. In addition to these studies, fuzzy logic controllers have also been integrated with the SMCs, where fuzzy logic is used for adaptation of the controller parameters. Some authors used fuzzy logic in order to tune the discontinuous control gain of the conventional SMC [28–30]. In another study, a fuzzy tuning approach where the sliding surface can rotate or shift in the phase space in such a direction that tracking behavior can be improved, was presented [31]. Noroozi et al. proposed an adaptive fuzzy sliding mode control scheme where discontinuous part of the control rule is obtained by a fuzzy unit and that part of the control rule includes an adaptive gain [32].

Rest of the paper is organized as follows: physical and mathematical models of the robot arms with the load were presented in Section 2. In Section 3, a robust non-chattering multiple-input multiple-output fuzzy sliding mode controller (MIMO-FSMC) was introduced to control the robot arms in trajectory tracking. Finally, performance of the proposed controller for the control of dual arm robots for load transportation in the presence of parameter variations and external disturbances was presented in Section 4 and concluding remarks were given in the last section.

## 2. Physical model

The planar dual arm robotic system consists of two arms and both arms have two degrees of freedom (DoF). Referring to Fig. 1, $m_i$, $I_i$ and $L_i$ are the mass, mass moment of inertia and length of the related links in physical model of the robot system, respectively, where $d_1$ is the width of the rectangular load and $d_2$ is the distance between the base of the robot arms. The distance of the mass center of the related link to the preceding joint and the joint angle of the related link are denoted as $k_i$ and $\theta_i$, respectively. Also, $b_i$ is used to denote the viscous frictions on all of the joints. The mass of the object $m(t)$ might change during the transportation. Actuating motors are also considered to be mounted on revolute joints. The numerical values of the parameters are given in the appendix.

The robot arms move in the horizontal $xy$-plane and gravity acts in the negative $z$-direction. There are two periods in the motion of the robots. First, robot arms start motion from their home positions and move towards the rectangular load. Then, in the second part, robot arms handle and transport the load to its new position by tracking the given trajectory. The robot applies forces $F_1$, $F_2$ from arm tips to the load to perform transportation task (Fig. 2). Friction forces $F_{s1}$, $F_{s2}$ and their components $F_{s1y}$, $F_{s1z}$, $F_{s2y}$, $F_{s2z}$ between arm tips and load surface prevent slipping of the load from the contact points during motion. Here $\mu$ represents the coefficient of dry friction. Since in this study it is aimed that the load is moved without rotation about the $z$-axis, $F_{s1y}$ and $F_{s2y}$ are specified as equal. Similarly, both $F_{s1z}$ and $F_{s2z}$ are equal to the half of the weight of the load since there is no rotation about the $y$-axis.

Since the position of the center of mass $(x_{m(t)}, y_{m(t)})$ is common in defining the trajectory of both arms, the DoF of the overall system reduces to two as presented:

$$x_{m(t)} = \frac{d_2}{2} + L_1\cos\theta_1 + L_2\cos(\theta_1+\theta_2) - \frac{d_1}{2} = -\frac{d_2}{2} + L_3\cos\theta_3 + L_4\cos(\theta_3+\theta_4) + \frac{d_1}{2} \tag{1}$$

$$y_{m(t)} = L_1\sin\theta_1 + L_2\sin(\theta_1+\theta_2) = L_3\sin\theta_3 + L_4\sin(\theta_3+\theta_4) \tag{2}$$

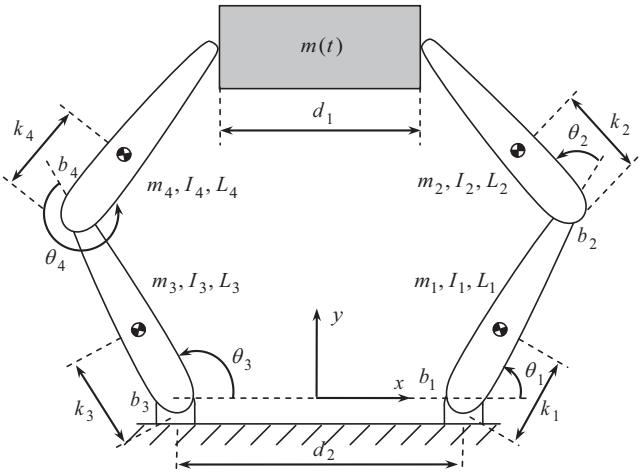


Fig. 1. Physical model of the robot arms.

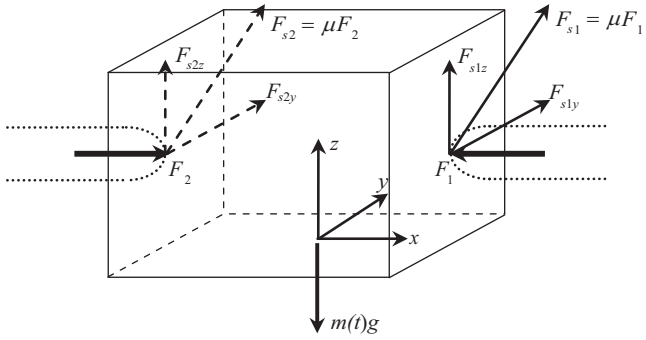


Fig. 2. The forces acting on the load.

Equations of motion for the robot arms when transporting the load are given in vector form as

$$[M(\theta)]\ddot{\theta} + \boldsymbol{C}(\theta,\dot{\theta}) = \boldsymbol{u} + [J]^T \boldsymbol{F} + \boldsymbol{T}_d \tag{3}$$

Here, $[M(\theta)]$ is a $4 \times 4$ mass matrix, $\boldsymbol{C}(\theta,\dot{\theta})$ is a $4 \times 1$ vector and includes the coriolis and centrifugal terms, $\boldsymbol{u}$ is a $4 \times 1$ control torque input vector, $\boldsymbol{F}$ is a $4 \times 1$ vector including interaction forces, $[J]$ is a $4 \times 4$ Jacobian matrix and $T_d$ is a $4 \times 1$ vector including the noise effects on robot arms. The details of Eq. (3) are given in the appendix. The motion equations of the load are

$$m(t)\,\ddot{x}_{m(t)} = F_2 - F_1 \tag{4}$$

$$m(t)\,\ddot{y}_{m(t)} = 2F_{s1y} = 2F_{s2y} \tag{5}$$

and the expressions for friction forces are

$$F_{s1y}{}^2 + \left(\frac{m(t)g}{2}\right)^2 < (\mu F_1)^2 \tag{6}$$

$$F_{s2y}{}^2 + \left(\frac{m(t)g}{2}\right)^2 < (\mu F_2)^2 \tag{7}$$

Since the direction of the forces $F_1$ and $F_2$ are determined to be towards the load in order to be able to handle the load, these forces should always be positive. Therefore, a friction force equation, giving positive signed solution for both $F_1$ and $F_2$, should be chosen. If $\ddot{x}_{m(t)} \geq 0$, then using Eq. (6) following relations for $F_1$ and $F_2$ are obtained:

$$F_1 = \frac{1}{\mu}\sqrt{\left(\frac{m\ddot{y}_{m(t)}}{2}\right)^2 + \left(\frac{m(t)g}{2}\right)^2} \tag{8}$$

$$F_2 = \frac{1}{\mu}\sqrt{\left(\frac{m(t)\ddot{y}_{m(t)}}{2}\right)^2 + \left(\frac{m(t)g}{2}\right)^2} + m(t)\ddot{x}_{m(t)} \tag{9}$$

Since $\ddot{x}_{m(t)} \geq 0$, the interaction forces $F_1$ and $F_2$ are both positive. If $\ddot{x}_{m(t)} < 0$, then Eq. (7) is used and following relations for the interaction forces are obtained:

$$F_1 = \frac{1}{\mu}\sqrt{\left(\frac{m(t)\ddot{y}_{m(t)}}{2}\right)^2 + \left(\frac{m(t)g}{2}\right)^2} - m(t)\ddot{x}_{m(t)} \tag{10}$$

$$F_2 = \frac{1}{\mu}\sqrt{\left(\frac{m\ddot{y}_{m(t)}}{2}\right)^2 + \left(\frac{m(t)g}{2}\right)^2} \tag{11}$$

Since $\ddot{x}_{m(t)} < 0$, the interaction forces $F_1$ and $F_2$ are both positive. Also it should be noted that by obtaining the interaction forces as described above it is also assured that the solution set, which results in small friction and interaction forces, is used.

## 3. MIMO fuzzy sliding mode controller design

In sliding mode controlled systems, states of the system are forced to reach a predefined sliding surface and then they are constrained to stay in the neighborhood of this surface [33]. In the sequel, states converge to the stable equilibrium point of the system which is generally the origin of the error phase plane [34].

The state space form of a nonlinear dynamic system can be written as

$$\boldsymbol{\phi} = \boldsymbol{f}(\boldsymbol{\phi}) + [B]\boldsymbol{u} \tag{12}$$

where $\boldsymbol{\phi} = [\phi_1, \ldots, \phi_n, \phi_{n+1}, \ldots, \phi_{2n}]^T$. The second half of the states are the time derivatives of the first half for mechanical systems, and $2n$ is the number of the states. In Eq. (12), $\boldsymbol{f}(\phi)$ is the $2n \times 1$ vector of the state equations without the control inputs, $\boldsymbol{u}$ is the $n \times 1$ generalized torque input vector and $[B]$ is $2n \times n$ matrix that its elements are the coefficients of the generalized control inputs in the state equations. For the first arm of the dual arm robot, by choosing the state variables as $[\phi_{1(1)}\phi_{2(1)}\phi_{3(1)}\phi_{4(1)}]^T = [\theta_1\theta_2\dot{\theta}_1\dot{\theta}_2]^T$ and the control input as $u_{(1)} = [u_1\, u_2]^T$, the equations of motion for the first arm can easily be arranged in the form of Eq. (12). Similarly, for the second robot arm defining the state variables as $[\phi_{1(2)}\phi_{2(2)}\phi_{3(2)}\phi_{4(2)}]^T = [\theta_3\theta_4\dot{\theta}_3\dot{\theta}_4]^T$ and the control input vector as $u_{(2)} = [u_3\, u_4]^T$ the equations of motion for the second robot arm can be arranged in the form of Eq. (12). Therefore, the controller design for the robot arms can be treated separately. Here, subscripts (1) and (2) in the state variables stand for the first and second robot arm, respectively.

The sliding surface is defined as follows:

$$S = \{\boldsymbol{\phi} : \boldsymbol{\sigma}(\phi, t) = 0\} \tag{13}$$

Hereafter, for the clarity of presentation, the arguments of the functions are omitted. For a control system, the sliding function can be selected as

$$\boldsymbol{\sigma} = [G]\boldsymbol{\Delta\phi} \tag{14}$$

Here

$$\boldsymbol{\Delta\phi} = \boldsymbol{\phi}_r - \boldsymbol{\phi} = \left[\boldsymbol{e}\, d\boldsymbol{e}/dt\right]^T \tag{15}$$

is the difference between the reference and actual system state vectors $\boldsymbol{\phi}_r$ and $\boldsymbol{\phi}$, respectively. The matrix $[G]$ includes the sliding surface slopes:

$$[G]=\begin{bmatrix} \lambda_1 & 0 & 0 & 0 & 0 & 1 & 0 & 0 & 0 & 0 \\ 0 & \ddots & 0 & 0 & 0 & 0 & \ddots & 0 & 0 & 0 \\ 0 & 0 & \lambda_i & 0 & 0 & 0 & 0 & 1 & 0 & 0 \\ 0 & 0 & 0 & \ddots & 0 & 0 & 0 & 0 & \ddots & 0 \\ 0 & 0 & 0 & 0 & \lambda_n & 0 & 0 & 0 & 0 & 1 \end{bmatrix}_{n\times 2n} \tag{16}$$

The slope parameter $\lambda_i$ represents the negative value of the each related sliding surface slope:

$$\sigma_i=\lambda_i e_i+\dot{e}_i=0 \tag{17}$$

For overall stability, the following Lyapunov function candidate has to be positive definite and its derivative has to be negative semi-definite:

$$\boldsymbol{v}=\frac{\boldsymbol{\sigma}^T\boldsymbol{\sigma}}{2}>0 \tag{18}$$

$$\frac{d\boldsymbol{v}}{dt}=\frac{\dot{\boldsymbol{\sigma}}^T\boldsymbol{\sigma}}{2}+\boldsymbol{\sigma}^T\frac{\dot{\boldsymbol{\sigma}}}{2}\leq 0 \tag{19}$$

If the limit condition is applied to Eq. (19), then

$$\frac{d\boldsymbol{\sigma}}{dt}=\frac{d\boldsymbol{A}}{dt}-[G]\frac{d\boldsymbol{\phi}}{dt}=0 \tag{20}$$

where

$$\boldsymbol{A}=[G]\boldsymbol{\phi}_r \tag{21}$$

From Eqs. (12) and (14),

$$\frac{d\boldsymbol{A}}{dt}-[G]\left(\boldsymbol{f}+[B]\boldsymbol{u}_{eq}\right)=0 \tag{22}$$

where $\boldsymbol{u}_{eq}$ is the equivalent control torque input vector for the limit case. Finally equivalent control is found as follows:

$$\boldsymbol{u}_{eq}=[GB]^{-1}\left(\frac{d\boldsymbol{A}}{dt}-[G]\boldsymbol{f}\right) \tag{23}$$

Equivalent control is valid only on the sliding surface. Thus, an additional term should be defined to pull the system to the surface. For this purpose, the derivative of the Lyapunov function along the system trajectories is selected to be as follows [21]:

$$\dot{\boldsymbol{v}}=-\boldsymbol{\sigma}^T[\Gamma]\boldsymbol{\sigma}<0 \tag{24}$$

By equating (19)–(24) and carrying out similar manipulations as in calculation of $u_{eq}$, the total control input is found as

$$\boldsymbol{u}=\boldsymbol{u}_{eq}+[GB]^{-1}[\Gamma]\boldsymbol{\sigma} \tag{25}$$

This total control input ensures that the derivative of the Lyapunov function along the system trajectories is as in Eq. (24). $[GB]^{-1}$ is always invertible and equal to mass matrix for mechanical systems. Here, $[\Gamma]$ is a positive definite diagonal matrix which includes the

control gains. However, if the knowledge of $f$ and $[B]$ are not well known, the equivalent calculated control inputs will be completely different from the actual equivalent control inputs. Thus, in this study, it is assumed that the equivalent control is the average of the total control [35,36]. For estimation of the equivalent control, an averaging filter, here a low pass filter can be designed as follows:

$$T\dot{\hat{\boldsymbol{u}}}_{eq} + \hat{\boldsymbol{u}}_{eq} = \boldsymbol{u} \tag{26}$$

The main idea, which is used in the design stage of the low pass filter, is based on that low frequencies determine the characteristics of the signal and high frequencies come from unmodeled dynamics. On the other hand, using such estimation minimizes the need for system

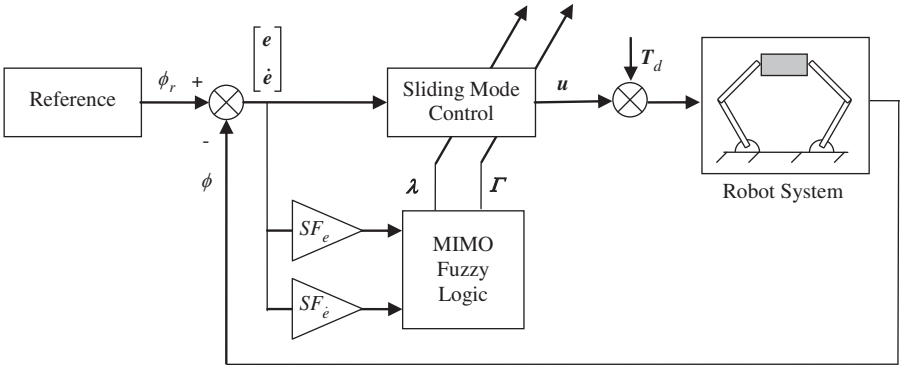


Fig. 3. MIMO fuzzy sliding mode controller (MIMO-FSMC) with adaptive slope and control gain.

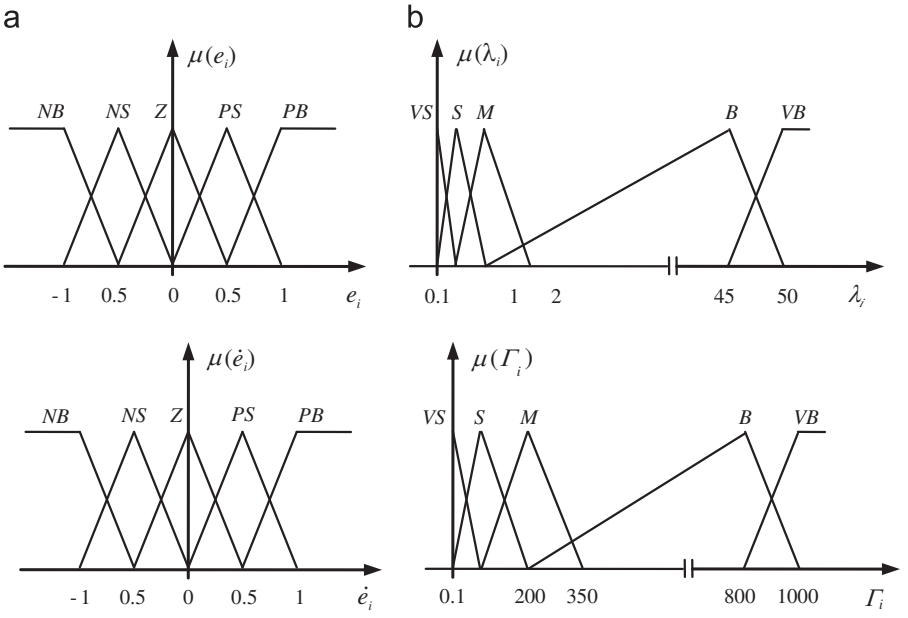


Fig. 4. Membership functions for (a) input variables and (b) output variables.

information for the control input calculation. Finally the non-chattering control input results in,

$$\boldsymbol{u} = \hat{\boldsymbol{u}}_{eq} + [GB]^{-1}[\Gamma]\boldsymbol{\sigma} \tag{27}$$

It is well known that sliding mode control is insensitive to parameter variations when the system states are on the sliding surface [33]. Thus, shortening the reaching time to surface improves the robust behavior of the controller [22]. In order to achieve this goal, the slope of the surface is tuned such that it does not wait for the states to reach it on its course but travels to them dynamically. Therefore, in this study, the slope parameters of the sliding surfaces are not constant but tuned by the MIMO fuzzy logic unit, which cause the system states to be caught by the sliding surface, earlier. Since the control gain of the SMC also has an effect on the reaching time to the sliding surface, in this study it is also updated by the MIMO fuzzy logic unit. Fig. 3 shows the general structure of the MIMO fuzzy sliding mode controller (MIMO-FSMC) with adaptive sliding surface slope and adaptive control gain.

As seen in Fig. 4, the triangular membership functions are used for the fuzzification of the inputs, which are error $e_i$ and derivative of error $\dot{e}_i$. The first output is slope parameter $\lambda_i$, which is the negative value of the related sliding surface slope. The second output is the control gain $\Gamma_i$. Input membership functions are defined on the [−1,1] closed interval. Thus, in order to map the crisp input variables to their fuzzy universe of discourse, scaling factors ($SF_e$,$SF_{\dot{e}}$) are used. The scaling factors for the input membership functions and, the range and locations of the output membership functions are found by trial at the design

Table 1
Rule table for the slope parameter $\lambda_i$ and control gain $\Gamma_i$.

| $e_i$ | $\dot{e}_i$ | | | | |
|---|---|---|---|---|---|
| | ***NB*** | ***NS*** | ***Z*** | ***PS*** | ***PB*** |
| ***NB*** | *M*(*M*) | *S*(*B*) | *VS*(*VB*) | *S*(*B*) | *M*(*M*) |
| ***NS*** | *B*(*S*) | *M*(*M*) | *S*(*B*) | *M*(*M*) | *B*(*S*) |
| ***Z*** | *VB*(*VS*) | *B*(*S*) | *M*(*M*) | *B*(*S*) | *VB*(*VS*) |
| ***PS*** | *B*(*S*) | *M*(*M*) | *S*(*B*) | *M*(*M*) | *B*(*S*) |
| ***PB*** | *M*(*M*) | *S*(*B*) | *VS*(*VB*) | *S*(*B*) | *M*(*M*) |

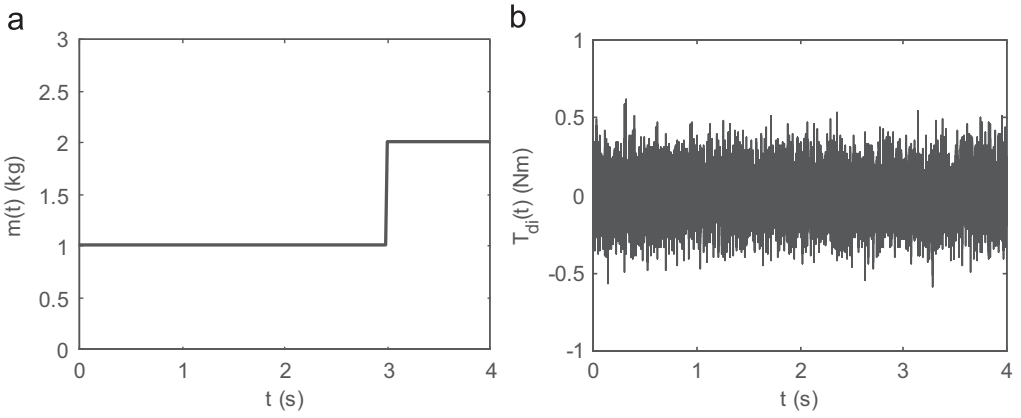


Fig. 5. (a) Change in load mass and (b) noise disturbance.

stage. Furthermore, at the design stage, it was concluded that, if all the membership functions overlap each other with 0.5° of membership, very small or very big values for the sliding surface slope and control gain could not be attained. Therefore, to be able to make surface slope value or control gain smaller or bigger whenever necessary, the locations of

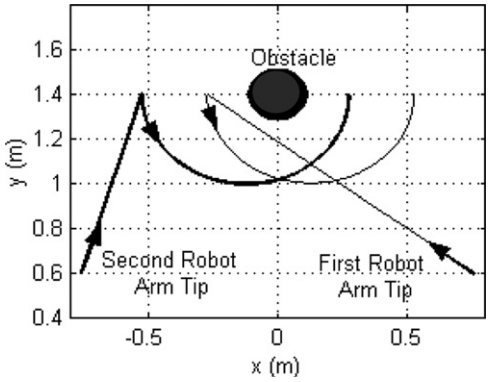


Fig. 6. Trajectories of the robot arm tips during approaching and transportation periods.

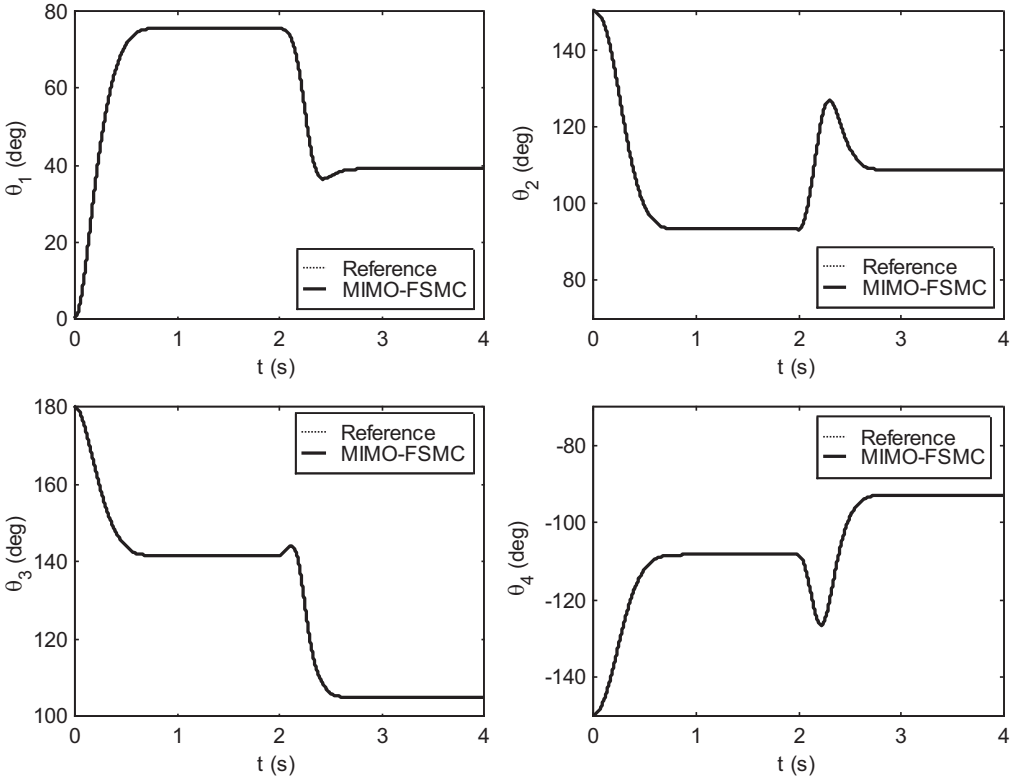


Fig. 7. The reference and the actual joint angles.

the output membership functions are arranged as seen in Fig. 4(b). The design parameters of the fuzzy sliding mode controller are given in the appendix.

If the differential Eq. (17) of the sliding surface is solved, it can be seen that, in order to have a stable motion on the sliding surface, each $\lambda_i$ must be positive. This implies that the sliding surface can only move through the second and fourth quadrants of the $e_i$ vs. $\dot{e}_i$ phase plane. Thus, the stability of the system when the states are on the sliding surface is guaranteed as long as the sliding surface moves through the stable regions of the phase plane. The rule table for $\lambda_i$ and $\Gamma_i$ is given in Table 1. In this table, the output membership functions in the parenthesis belong to the update rules for the control gain $\Gamma_i$ and the membership functions out of the parenthesis belong to the update rules for the slope parameter $\lambda_i$. For example, if $e_i$ is $PS$ and $\dot{e}_i$ is $NB$ then $\lambda_i$ is $B$ and $\Gamma_i$ is $S$. The logic behind this rule table is to make the sliding surfaces move towards the error states, and at the same time to force the states to reach the surface faster, resulting in more successful and precise trajectory tracking than the conventional approaches.

## 4. Results and discussion

In order to test the robust behavior of the proposed controller, an unexpected load change is introduced during the transportation motion. This sudden change in load mass is

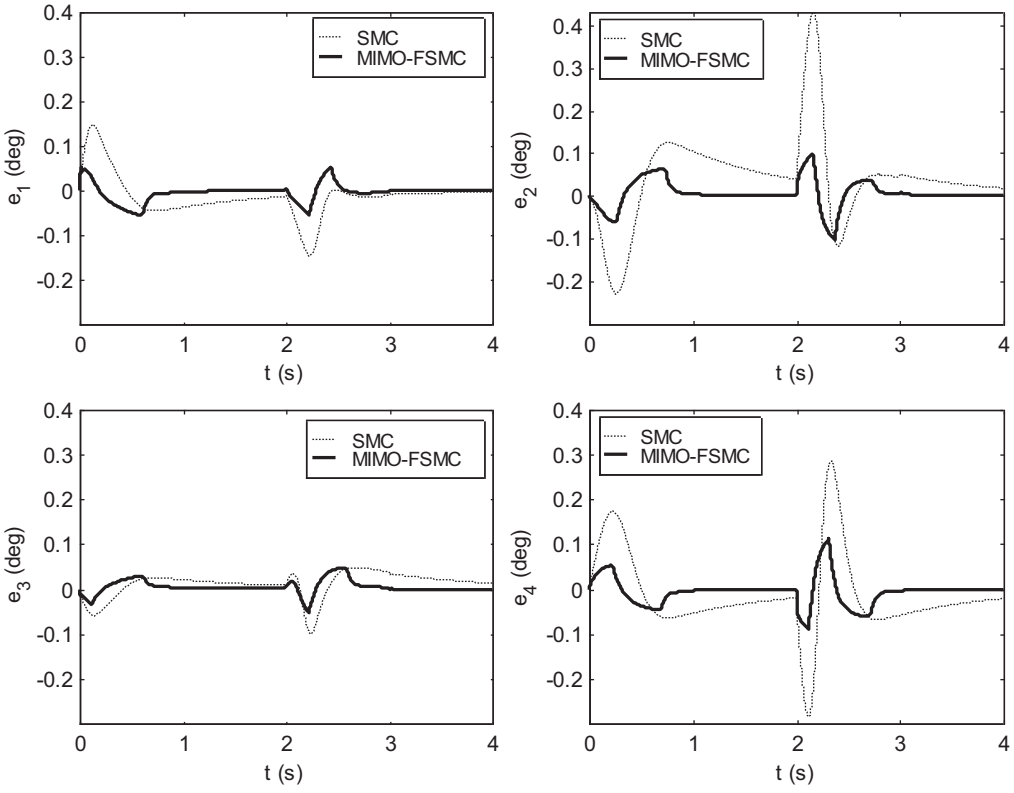


Fig. 8. Comparison of the tracking errors of the related joint angles.

introduced after third second as shown in Fig. 5(a). In addition, to test the insensitivity of the proposed controller to external disturbances, the joints are subjected to normally distributed noise components which are thought as random disturbing torques (Fig. 5(b)). The external disturbance torques act on every joint during the whole motion of the robot arms.

There are two stages in the motion of the robot arms, namely approaching and transportation. Initially the robot arms are at rest and the corresponding initial values of the joint angles are $\theta_1(0)=0$, $\theta_2(0)=5\pi/6$, $\theta_3(0)=\pi$ and $\theta_4(0)=-5\pi/6$. In the first part of the motion, the robot arms approach to the load and in the second part, the robot arms handle the load and transport it to its new location. The reference trajectories of the robot arm tips for approaching motion are defined in Eqs. (28) and (29). In addition, there exists a stationary obstacle between the initial and final positions of the load thus, a circular reference trajectory is preferred during load transportation for a smooth movement. The reference trajectories for the coordinates of the load center during the transportation are defined in Eqs. (30)–(32):

$$x_{mr}(t) = x_f + (x_i - x_f)\exp(-10t^2) \tag{28}$$

$$y_{mr}(t) = y_f + (y_i - y_f)\exp(-10t^2) \tag{29}$$

$$x_{mr}(t) = x_{ro} + r_r \cos\psi_r(t) \tag{30}$$

$$y_{mr}(t) = y_{ro} + r_r \sin\psi_r(t) \tag{31}$$

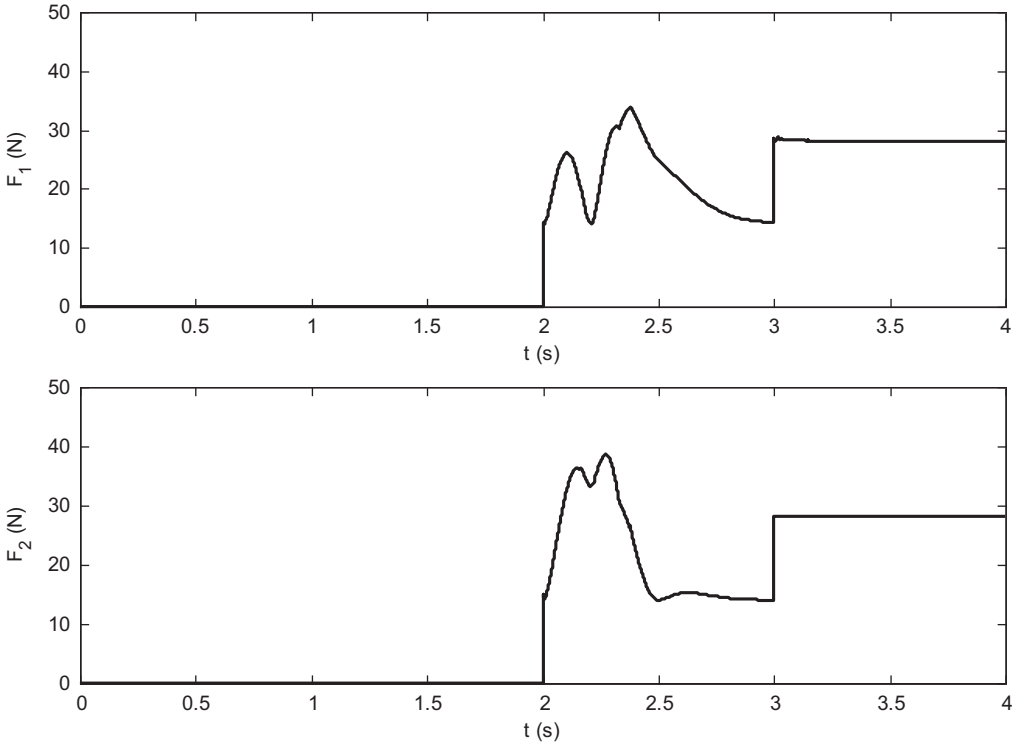


Fig. 9. Interaction forces.

$$\psi_r(t) = \psi_{rf} + (\psi_{ri} - \psi_{rf})\exp(-10(t-2)^2) \tag{32}$$

Here, $(x_i,y_i)$ and $(x_f,y_f)$ are initial and final coordinates of robot arm tips for approaching motion, $(x_{r0},y_{r0})$ is center of the circular trajectory with radius $r_r$ for transportation motion. The numerical values of the parameters of trajectories are given in the appendix. The approaching motion finishes at 2nd second and the transportation starts after that time. The actual trajectories of the robot arm tips realized by the designed controller during approaching and transportation phases are given in Fig. 6.

Using inverse kinematics with the given trajectory of the load, the reference angles for the controllers are obtained. These reference angles and the actual MIMO fuzzy sliding mode controlled joint angles are given in Fig. 7. It is seen from this figure that both robot arms track their trajectory successfully since the reference and actual angle values overlap.

Fig. 8 shows the tracking errors for the related joint angles. For the purpose of comparison, the tracking errors for the sliding mode controlled dual arm robot are also included in this figure. It is observed that for all of the joints, the maximum tracking error magnitudes are below 0.5° and these error values converge to zero rapidly. Also, it should be noted that there are no apparent changes in the magnitude of errors after the unexpected load variation at third second, which indicate the success of the SMC and the proposed MIMO-FSMC. Additionally, it is observed from this figure that with MIMO-FSMC the tracking error magnitudes are smaller and converge faster to zero if compared with the sliding mode controlled case.

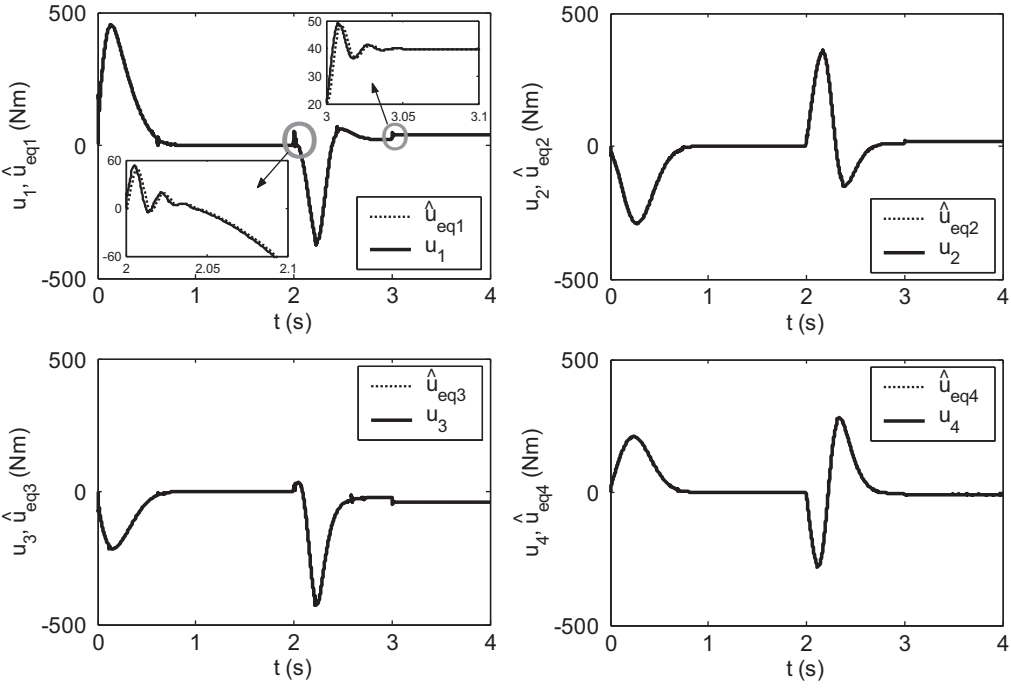


Fig. 10. Joint torques produced by proposed controller.

The variations of the magnitudes of the interaction forces $F_1$ and $F_2$ vs. time are given in Fig. 9. Both forces have zero magnitudes on time interval [0,2] since there is no interaction between the load and the robot arms during the approaching motion. Then, in the second part of the motion, the load is handled and forces start to act. There are apparent changes in the magnitudes of these forces after third second. This is due to the unexpected load variation. At the end of the motion, it is observed that there exist residual forces for both $F_1$ and $F_2$ which are due to the weight of the load. In fact the sum of these residual forces is equal to $m(t)g/\mu$.

The control input torques, which are produced by MIMO-FSMC and acting on the related joints, are shown in Fig. 10. The changes in the torque magnitudes at $t=2$ s is due to the load handling which produces interaction forces at the contact points between the load and the tip of the robot arms. The desired non-chattering control is achieved during the approaching and transportation tasks as a result of proposed MIMO-FSMC. In Fig. 10, estimated equivalent control inputs are also superimposed on the total control inputs. It is seen that the total control inputs almost agree with the estimated equivalent control inputs, which are valid on the sliding surface. Therefore the results indicate that the proposed controller forces the system states to reach the sliding mode very fast.

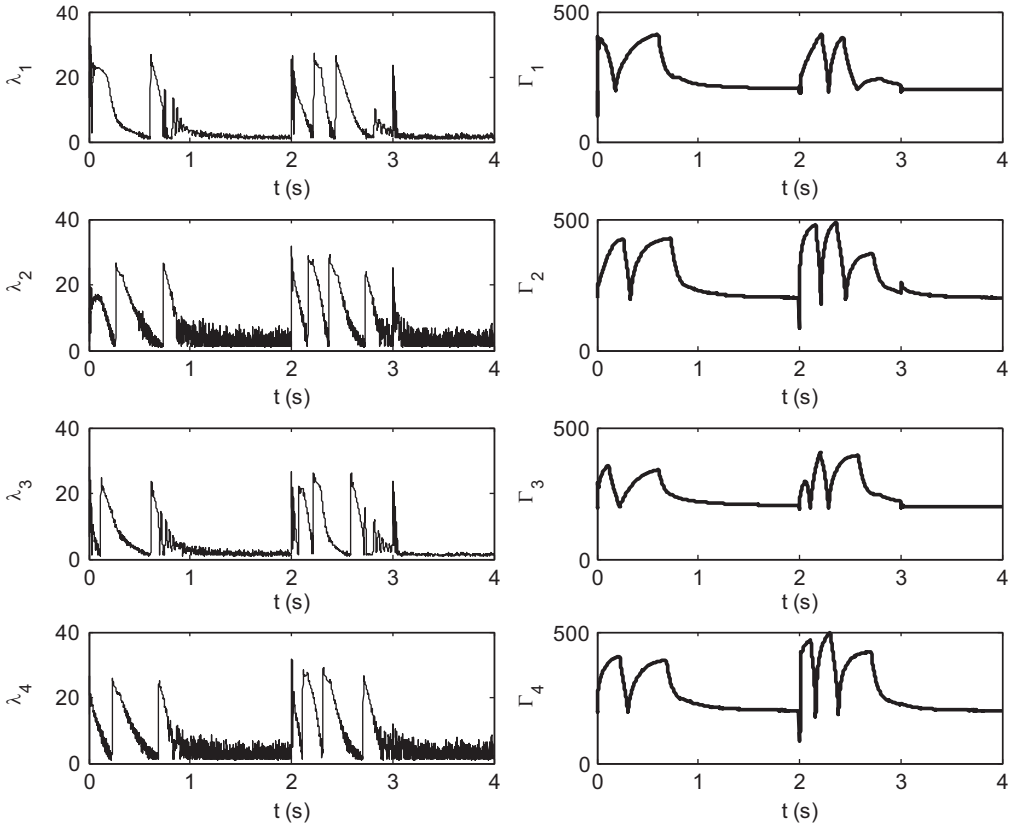


Fig. 11. Variations of the slope parameters and control gains of the proposed controller.

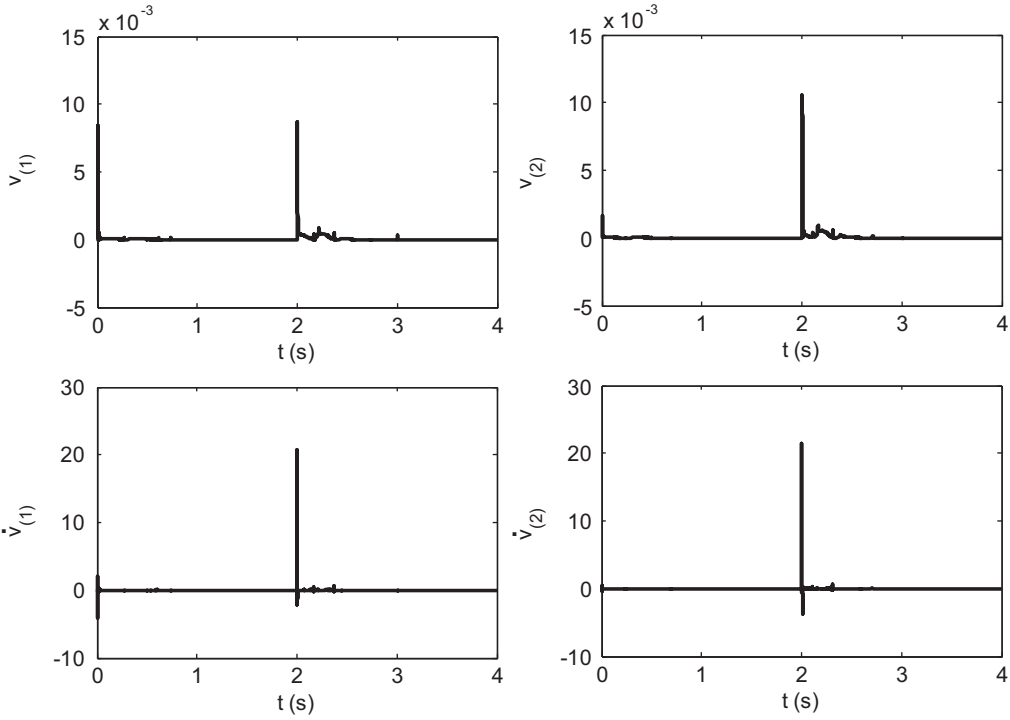


Fig. 12. Variation of the Lyapunov functions and their time derivatives for the first and second robot arms.

Fig. 11 shows the outputs of the fuzzy part of the controller which are the slope parameters of the sliding surface and control gains of the controller. It is seen that those parameters are tuned by the MIMO-fuzzy unit according to the error states of system which result in faster convergence to the sliding mode.

Variation of the Lyapunov functions ($v_{(1)}$,$v_{(2)}$) and their time derivatives ($\dot{v}_{(1)}$,$\dot{v}_{(2)}$) for the first and second robot arms are shown in Fig. 12. Here, subscripts (1) and (2) stand for the first and second robot arm, respectively. It is observed from this figure that at the beginning of the approaching and transportation motions, the Lyapunov functions increase for a short time duration and then converge to zero. The increase in Lyapunov functions is also reflected in their time derivatives where they take positive values for short durations of time. This is due to insufficient control energy available to construct a sliding motion at the beginning of approaching and transportation motions. On the other hand, it is seen that by tuning the slope constant and control gain of the sliding mode controller using proposed MIMO-fuzzy logic unit, the proposed controller recovers very fast and regulates the Lyapunov function and its derivative to zero.

## 5. Conclusion

In this study, in order to meet the accuracy and safety requirements of load transportation in hazardous environments, a robust non-chattering MIMO fuzzy sliding

mode control method was proposed. In this controller the slope constant and the control gain of the sliding mode controller are both updated at the same time via a MIMO fuzzy logic unit. In terms of trajectory tracking capability it was verified that proposed MIMO-FSMC showed a better performance than the SMC. Furthermore, it was seen from the tracking error values of the joint angles that proposed control method was able to overcome the unexpected, sudden load variation and normally distributed noise components during transportation operation. It is expected that this control method would be applicable to various mechanical systems that require more motion capability and complex design.

## Appendix

(i) Numerical parameters of the dual arm robot:

| | | |
|---|---|---|
| $m_i = 1.5$ (kg) | $k_i = 0.48$ (m) | $bi = 110$ (N m s) |
| $I_i = 0.18$ (kg m$^2$) | $\mu = 0.35$ | $d1 = 0.25$ (m) |
| $L_i = 1.2$ (m) | $m(t) =$ (see Fig. 5a) | $d2 = 1.2$ (m) |

$i = 1,2,3,4$

(ii) The vectors and matrices used in the equation of motion of the robot arms:

$$\mathbf{u} = \begin{bmatrix} u_1 & u_2 & u_3 & u_4 \end{bmatrix}^T, \quad \boldsymbol{F} = \begin{bmatrix} F_1 & F_{s1y} & F_2 & F_{s2y} \end{bmatrix}^T \boldsymbol{T}_d = [T_{d1} \quad T_{d2} \quad T_{d3} \quad T_{d4}]^T$$

$$[M(\theta)] = \begin{bmatrix} A_1 + A_2 + 2A_3\cos\theta_2 & A_2 + A_3\cos\theta_2 & 0 & 0 \\ A_2 + A_3\cos\theta_2 & A_2 & 0 & 0 \\ 0 & 0 & A_4 + A_5 + 2A_6\cos\theta_4 & A_5 + A_6\cos\theta_4 \\ 0 & 0 & A_5 + A_6\cos\theta_4 & A_5 \end{bmatrix}$$

$$\boldsymbol{C}(\theta,\dot{\theta}) = \begin{bmatrix} -A_3\sin\theta_2(\dot{\theta}_2^2 + \dot{\theta}_1\dot{\theta}_2) + b_1\dot{\theta}_1 \\ A_3\dot{\theta}_1^2\sin\theta_2 + b_2\dot{\theta}_2 \\ -A_6\sin\theta_4(\dot{\theta}_4^2 + \dot{\theta}_3\dot{\theta}_4) + b_3\dot{\theta}_3 \\ A_6\dot{\theta}_3^2\sin\theta_4 + b_4\dot{\theta}_4 \end{bmatrix}$$

$$[J]^T = \begin{bmatrix} -L_1\sin\theta_1 - L_2\sin(\theta_1+\theta_2) & -L_1\cos\theta_1 - L_2\cos(\theta_1+\theta_2) & 0 & 0 \\ -L_2\sin(\theta_1+\theta_2) & -L_2\cos(\theta_1+\theta_2) & 0 & 0 \\ 0 & 0 & L_3\sin\theta_3 + L_4\sin(\theta_3+\theta_4) & -L_3\cos\theta_3 - L_4\cos(\theta_3+\theta_4) \\ 0 & 0 & L_4\sin(\theta_3+\theta_4) & -L_4\cos(\theta_3+\theta_4) \end{bmatrix}$$

The term used in the equations of motion of the robot arms:

$$K_1 = m_1{k_1}^2 + m_2{L_1}^2 + I_1, \quad K_4 = m_3{k_3}^2 + m_4{L_3}^2 + I_3$$
$$K_2 = m_2{k_2}^2 + I_2, \quad K_5 = m_4{k_4}^2 + I_4$$
$$K_3 = m_2L_1k_2, \quad K_6 = m_4L_3k_4$$

(iii) Numerical parameters of the controllers:

| | SMC | MIMO-FSMC |
|---|---|---|
| $\tau_i$ | 0.0011 | 0.0011 |
| $\Gamma_i$ | 200 | Determined by MIMO fuzzy logic |
| $\lambda_i$ | 1 | Determined by MIMO fuzzy logic |
| $SF_{ei}$ | – | 100 |
| $SF_{\dot{e}_i}$ | – | 5 |

$i=1,2,3,4$

(iv) Numerical parameters for the trajectories:

| | |
|---|---|
| $(x_{i(1)},y_{i(1)})=(0.76,0.6)$ (m) | $x_{ro}=0$ (m) |
| $(x_{i(2)},y_{i(2)})=(-0.76,0.6)$ (m) | $y_{ro}=1.4$ (m) |
| $(x_{f(1)},y_{f(1)})=(-0.275,1.4)$ (m) | $r_r=0.4$ (m) |
| $(x_{f(2)},y_{f(2)})=(-0.525,1.4)$ (m) | $\psi_{ri}=-\pi$ |
| | $\psi_{rf}=0$ |

Subscripts (1) and (2) denote the first and second robot arms, respectively.

## References


[1] K. Laroussi, H. Hemami, R.E. Goddard, Coordination of two planar robots in lifting, IEEE Journal of Robotics and Automation 4 (1) (1988) 77–85.

[2] Y.H. Liu, S. Arimoto, Distributively controlling two robots handling an object in the task space without any communication, IEEE Transactions on Automatic Control 41 (8) (1996) 1193–1198.

[3] J.F. Liu, K. Abdel-Malek, Robust control of planar dual-arm cooperative manipulators, Robotics and Computer-Integrated Manufacturing 16 (2–3) (2000) 109–120.

[4] A. Nagchaudhuri, D.P. Garg, Adaptive control and impedance control for dual robotic arms manipulating a common heavy load, in: Proceedings of the International Conference on Advanced Intelligent Mechatronics, Italy, 2001, pp. 683–688.

[5] W. Yim, M. Selvarajan, W.R. Wells, Sliding mode cooperative motion control of dual arm manipulators, Artificial Life and Robotics 3 (1999) 166–169.

[6] D. Khalili, M. Zomlefer, An intelligent robotic system for rehabilitation of joints and estimation of body segment parameters, IEEE Transactions on Biomedical Engineering 35 (2) (1988) 138–146.

[7] W. Meier, J. Graf, A two-arm robot system based on trajectory optimization and hybrid control including experimental evaluation, in: Proceedings of the IEEE International Conference on Robotics and Automation, USA, 1991, pp. 2618–2623.

[8] Q. Xue, A.A. Maciejewski, P.C.-Y. Sheu, Determining the collision-free joint space graph for two cooperating robot manipulators, IEEE Transactions on Systems, Man, and Cybernetics 23 (1) (1993) 285–294.

[9] M. Yamano, J.S. Kim, A. Konno, M. Uchiyama, Cooperative control of a 3D dual-flexible-arm robot, Journal of Intelligent and Robotic Systems 39 (2004) 1–15.

[10] C.R. Carignan, D.L. Akin, Cooperative control of two arms in the transport of an inertial load in zero gravity, IEEE Transactions on Robotics and Automation 4 (4) (1988) 414–419.

[11] A. Kron, G. Schmidt, Haptic telepresent control technology applied to disposal of explosive ordnances: principles and experimental results, in: Proceedings of the IEEE International Symposium on Industrial Electronics, Croatia, 2005, pp. 1505–1510.

[12] A. Cavallo, C. Natale, High-order sliding control of mechanical systems: theory and experiments, Control Engineering Practice 12 (2004) 1139–1149.

[13] P. Muraca, P. Pugliese, A variable-structure regulator for robotic systems, Automatica 33 (7) (1997) 1423–1426.
[14] Y. Tang, Terminal sliding mode control for rigid robots, Automatica 34 (1) (1998) 51–56.
[15] S. Yannier, A. Sabanovic, A. Onat, M. Bastan, Sliding mode based obstacle avoidance and target tracking for mobile robots, in: Proceedings of the IEEE International Symposium on Industrial Electronics, Croatia, 2005, pp. 1489–1494.
[16] E.M. Jafarov, R. Tasaltin, Robust sliding mode control for the uncertain MIMO aircraft model F-18, IEEE Transactions on Aerospace and Electronic Systems 36 (4) (2000) 1127–1141.
[17] V.I. Utkin, Sliding mode control design principles and applications to electric drives, IEEE Transactions on Industrial Electronics 40 (1) (1993) 23–36.
[18] E.A. Tannuri, A.C. Agostinho, H.M. Morishita, L. Moratelli Jr., Dynamic positioning systems: an experimental analysis of sliding mode control, Control Engineering Practice 18 (10) (2010) 1121–1132.
[19] N. Orani, A. Pisano, E. Usai, Fault diagnosis for the vertical three-tank system via high-order sliding-mode observation, Journal of the Franklin Institute 347 (6) (2010) 923–939.
[20] K.D. Young, V.I. Utkin, U. Ozguner, A control engineer's guide to sliding mode control, IEEE Transactions on Control Systems Technology 7 (3) (1999) 328–342.
[21] N. Yagiz, Alternative approaches in sliding mode control theory, in: Proceedings of the Second International Symposium on Mechanical Vibrations, Pakistan, 2000, pp. 94–103.
[22] S.B. Choi, C.C. Cheong, D.W. Park, Moving switching surfaces for robust control of second-order variable structure systems, International Journal of Control 58 (1) (1993) 229–245.
[23] R.G. Roy, N. Olgac, Robust nonlinear control via moving sliding surfaces—*n*th order case, in: Proceedings of the 36th Conference on Decision and Control, USA, 1997, pp. 943–948.
[24] S. Tokat, I. Eksin, M. Guzelkaya, M.T. Soylemez, Design of a sliding mode controller with a nonlinear time-varying sliding surface, Transactions of the Institute of Measurement and Control 25 (2) (2003) 145–162.
[25] A. Bartoszewicz, A. Nowacka-Leverton, SMC without the reaching phase—the switching plane design for the third-order system, IET Control Theory & Applications 1 (5) (2007) 1461–1470.
[26] S. Tokat, Sliding mode controlled bioreactor using a time varying sliding surface, Transactions of the Institute of Measurement and Control 31 (5) (2009) 435–456.
[27] A. Bartoszewicz, A. Nowacka-Leverton, ITAE optimal sliding modes for third-order systems with input signal and state constraints, IEEE Transactions on Automatic Control 55 (8) (2010) 1928–1932.
[28] Y. Guo, P.Y. Woo, Adaptive fuzzy sliding mode control for robotic manipulators, in: Proceedings of the 42nd IEEE Conference on Decision and Control, USA, 2003, pp. 2174–2179.
[29] C.M. Lin, Y.J. Mon, Hybrid adaptive fuzzy controllers with application to robotic systems, Fuzzy Sets and Systems 139 (2003) 151–165.
[30] S.B. Choi, J.S. Kim, A fuzzy-sliding mode controller for robust tracking of robotic manipulators, Mechatronics 7 (2) (1997) 199–216.
[31] Q.P. Ha, D.C. Rye, H.F.D. Whyte, Fuzzy moving sliding mode control with application to robotic manipulators, Automatica 35 (4) (1999) 607–616.
[32] N. Noroozi, M. Roopaei, M.Z. Jahromi, Adaptive fuzzy sliding mode control scheme for uncertain systems, Communications in Nonlinear Science and Numerical Simulation 14 (11) (2009) 3978–3992.
[33] C. Edwards, S.K. Spurgeon, Sliding Mode Control: Theory and Applications, Taylor & Francis, 1998.
[34] J.Y. Hung, W. Gao, J.C. Hung, Variable structure control: a survey, IEEE Transactions on Industrial Electronics 40 (1) (1993) 2–22.
[35] M. Ertugrul, O. Kaynak, A. Sabanovic, A comparison of various VSS techniques on the control of automated guided vehicles, in: Proceedings of the IEEE International Symposium on Industrial Electronics, Greece, 1995, pp. 837–842.
[36] V. Utkin, J. Guldner, J. Shi, Sliding Mode Control in Electromechanical Systems, Taylor & Francis, Padstow, 1999.